

Supplemental Materials: A Chiral, Incommensurate Helical Phase in a Smectic of Achiral Bent-Core Mesogens

Adam A. S. Green,¹ Michael R. Tuchband,¹ Renfan Shao,¹ Yongqiang Shen,¹ Rayshan Visvanathan,¹ Alexandra E. Duncan,¹ Anne Lehmann,² Carsten Tschiesske,² Eric D. Carlson,³ Edward Guzman,³ Maria Kolber,³ David M. Walba,³ Cheol S. Park,¹ Matthew A. Glaser,¹ Joseph E. MacLennan,¹ and Noel A. Clark¹

¹*Department of Physics and Soft Materials Research Center,
University of Colorado Boulder, Boulder, CO, 80309-0390, USA*

²*Department of Chemistry, Martin Luther University Halle-Wittenberg, D-06120 Halle, Germany*

³*Department of Chemistry and Soft Materials Research Center,
University of Colorado Boulder, Boulder, CO, 80309-0215, USA*

(Dated: February 12, 2019)

I. EXPERIMENTAL METHODS

We used a combination of two-dimensional, small-angle, hard X-ray scattering (SAXS), resonant, soft X-ray scattering (RSoXS), polarized, transmitted light microscopy on cells in transmission, and measurements of the polarization reversal current of cells in order to characterize **PAL30**.

The RSoXS experiments were performed at the Advanced Light Source at Lawrence Berkeley National Laboratory beamline 11.0.1.2 using linearly polarized X-ray photons [1, 2]. The X-ray energy was tuned between 270 eV and 290 eV in our experiments, with scattering contrast appearing only for energies near the carbon K-edge resonance ($E = 284$ eV), indicating the presence of real-space features with an orientational modulation. The **PAL30** material was sandwiched between two silicon nitride substrates, while in the isotropic phase. The cell was then placed into a temperature controlled hotstage in the beamline. After finding the highest temperature where scattering features were observed, the sample was cooled slowly while recording 2D diffractograms of the scattering. The RSoXS setup is sensitive to orientational modulations from $d = 50$ Å to 1250 Å. The relative positions and orientations of the sample and detector were calibrated using a sample with known scattering q -values. The data from the detector was processed using the Igor Pro-based NIKA data reduction software package [3, 4].

The angular resolution of the diffractometer, estimated from the full width at half-maximum of a resonant feature known to be twice the smectic layer spacing is $\delta q \sim 0.00078 \text{ \AA}^{-1}$.

SAXS measurements were carried out on beamline X10A of the National Synchrotron Light Source (NSLS), at Brookhaven National Laboratory. This beamline has a Si 111 double monochromator, tuned to around 10 keV. The sample was mounted in an Instec hot stage on a Huber four-circle goniometer. The angular resolution of the diffractometer, measured by scanning the detector arm through the attenuated direct beam, is $\delta q \sim 0.005 \text{ nm}^{-1}$ full width at half-maximum.

The planar cells used for texture analysis were 4.5 μm thick commercial cells purchased from Instec Inc. with rubbed polyimide planar alignment layers and ITO glass. The thickness of the empty cells was measured using a visible light spectrometer. The cells were then filled with **PAL30** in the isotropic phase. Polarization reversal current was measured in these cells by applying an alternating, triangular voltage.

The birefringence was measured using a Zeiss quartz-wedge compensator and a 5.86 μm thick Instec cell.

The molecular length of **PAL30** was estimated using a Hartree-Fock 6-31G* calculation of a single molecule in the gas phase using the Spartan 16 numerical calculation package.

II. SUPPLEMENTAL FIGURES

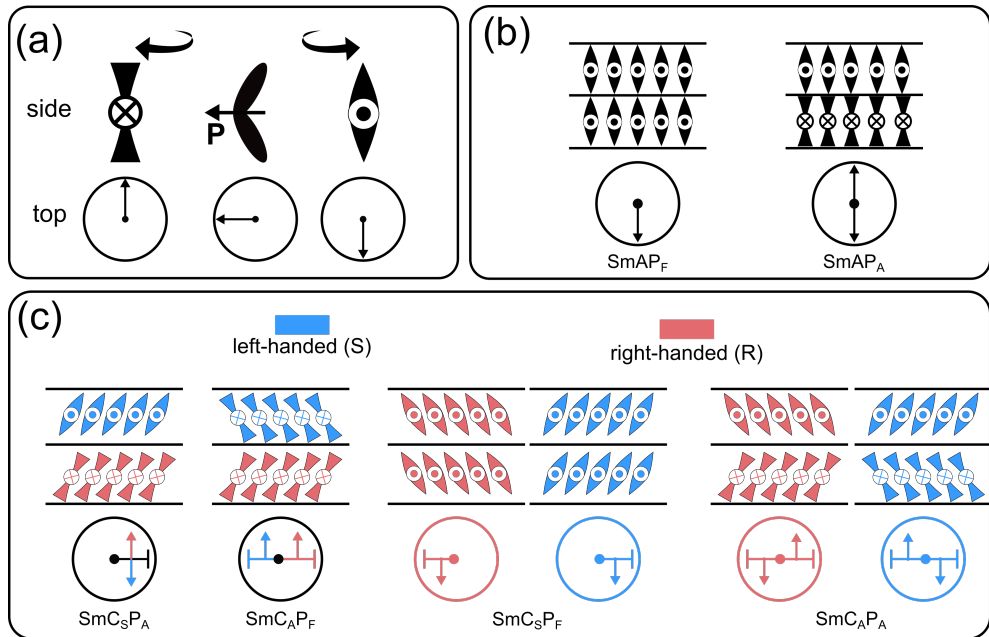


FIG. S1. Tilt and polarity of selected bent-core smectic phases. (a) Generic bent-core molecule at various orientations. (b) Polar orthogonal phases. (c) Tilted states of the B2 phase. The tilt director is indicated by \dashv and the polar vector by \rightarrow . The smectic layers are colored according to their chirality, with black being achiral or racemic, blue left-handed, and red right-handed.

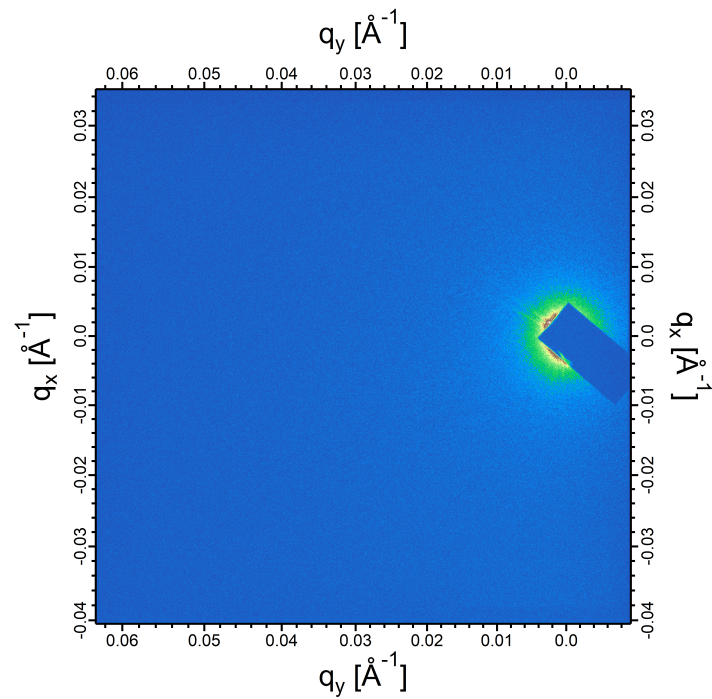


FIG. S2. Resonant soft X-ray scattering (RSoXS) of **PAL30** observed in the Sm1 phase ($T = 113^\circ\text{C}$). This image is characteristic of the phase. The absence of any resonant scattering features is characteristic of the Sm1 showing that there are no periodic structures present.

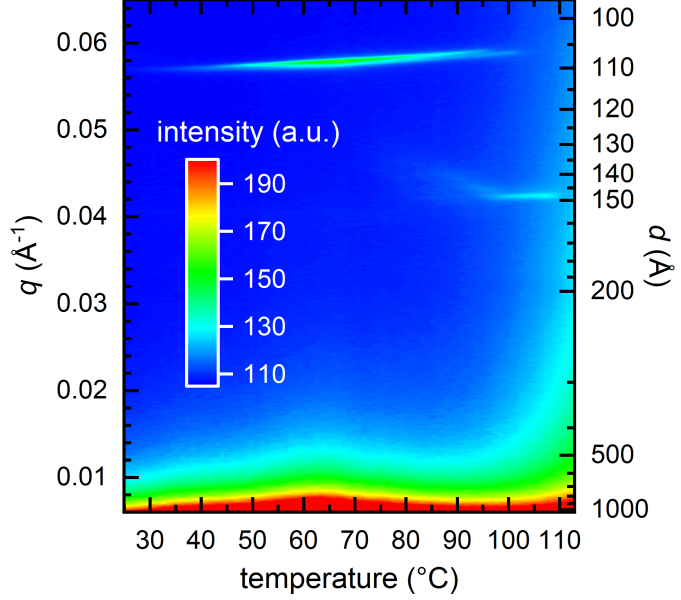


FIG. S3. Resonant soft X-ray scattering (RSoSXS) of **PAL30** observed vs. temperature on cooling. The plot was generated from a temperature series of 2D diffractograms that were azimuthally averaged, then interpolated and plotted in q -space with corresponding real-space coordinates ($d = 2\pi/q$). Above 110 °C, we observe no scattering features, indicating the absence of resonant structures periodic in this d -range. On cooling below 110 °C, a scattering arc appears at $d = 148 \text{ \AA}$, corresponding to about three smectic layer spacings. This reflection persists on further cooling but becomes weaker and disappears at 99 °C. At 105 °C, a second feature appears (at $d = 107 \text{ \AA}$) corresponding to two smectic layer spacings. This feature shifts to smaller q , and then disappears at the transition to the crystal phase at 65 °C. In the q range we investigated (corresponding to 50 \AA to 1256 \AA), we see no other orientational modulations.

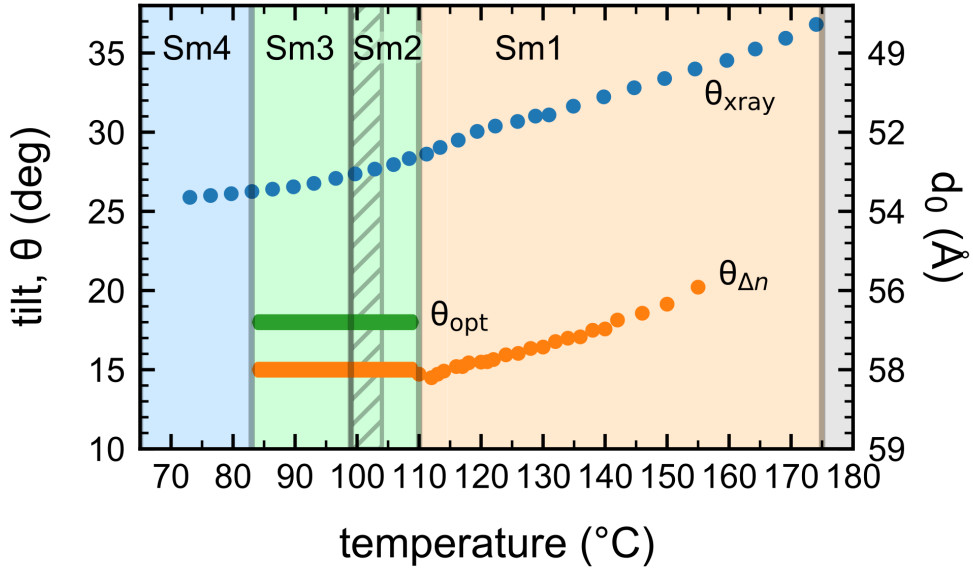


FIG. S4. Molecular tilt of **PAL30** as a function of temperature. The X-ray tilt is found using, $\theta_{xray} = \arccos(d_0/l_{calc})$, where d_0 is the smectic layer spacing measured by SAXS and $l_{calc} = 59.9 \text{ \AA}$ is the fully-trans calculated length from Spartan. The layer spacing (X-ray tilt) increases (decreases) monotonically on cooling. Even the highest value for the layer spacing ($d_0 \approx 54 \text{ \AA}$), is still significantly less than the predicted molecular length $l_{calc} = 59.9 \text{ \AA}$, suggesting that there may be a significant degree of intercalation or tilt present in all smectic phases. The fact that the Sm2 is chiral suggests that Sm2 *must* be tilted. Because the dramatic changes of the layer spacing that would be expected at a transition between an orthogonal and a tilted phase are not seen anywhere in the SAXS temperature scan, every smectic phase should also show comparable tilt. The fact that the measured optical tilt (θ_{opt}) is less than the tilt calculated from the layer spacing, θ_{xray} suggests a significant degree of intercalation is also present.

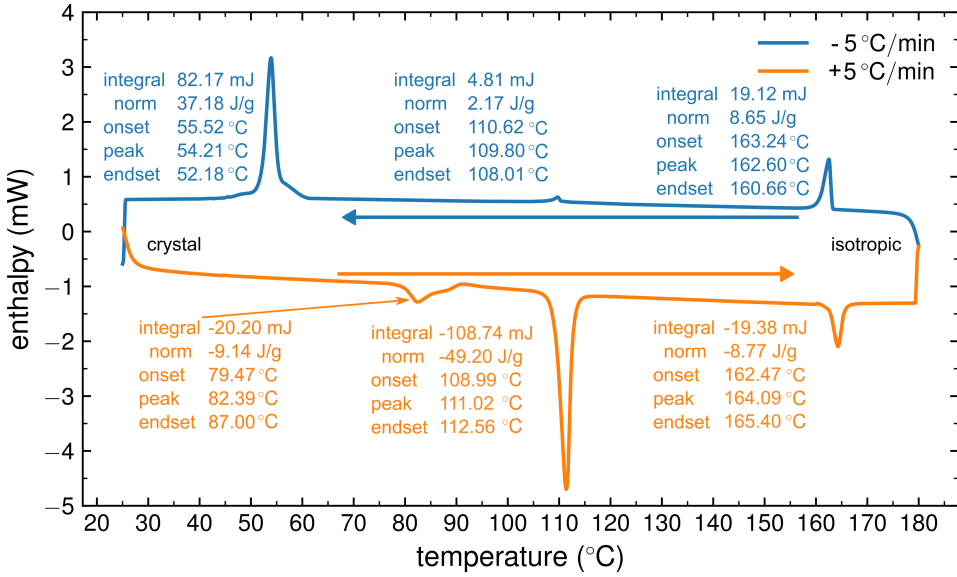


FIG. S5. Differential scanning calorimetry (DSC) of **PAL30** on slow cooling and heating. Since **PAL30** appears to be monotropic, all experimental characterization described in this paper was carried out on cooling, between the clearing point (162 °C) and crystallization (54.21 °C). The peak observed on cooling at 109.8 °C corresponds to the transition from the de Vries SmA to the Sm(CP)_α phase. The enthalpy of the other transitions was too small to be detected.

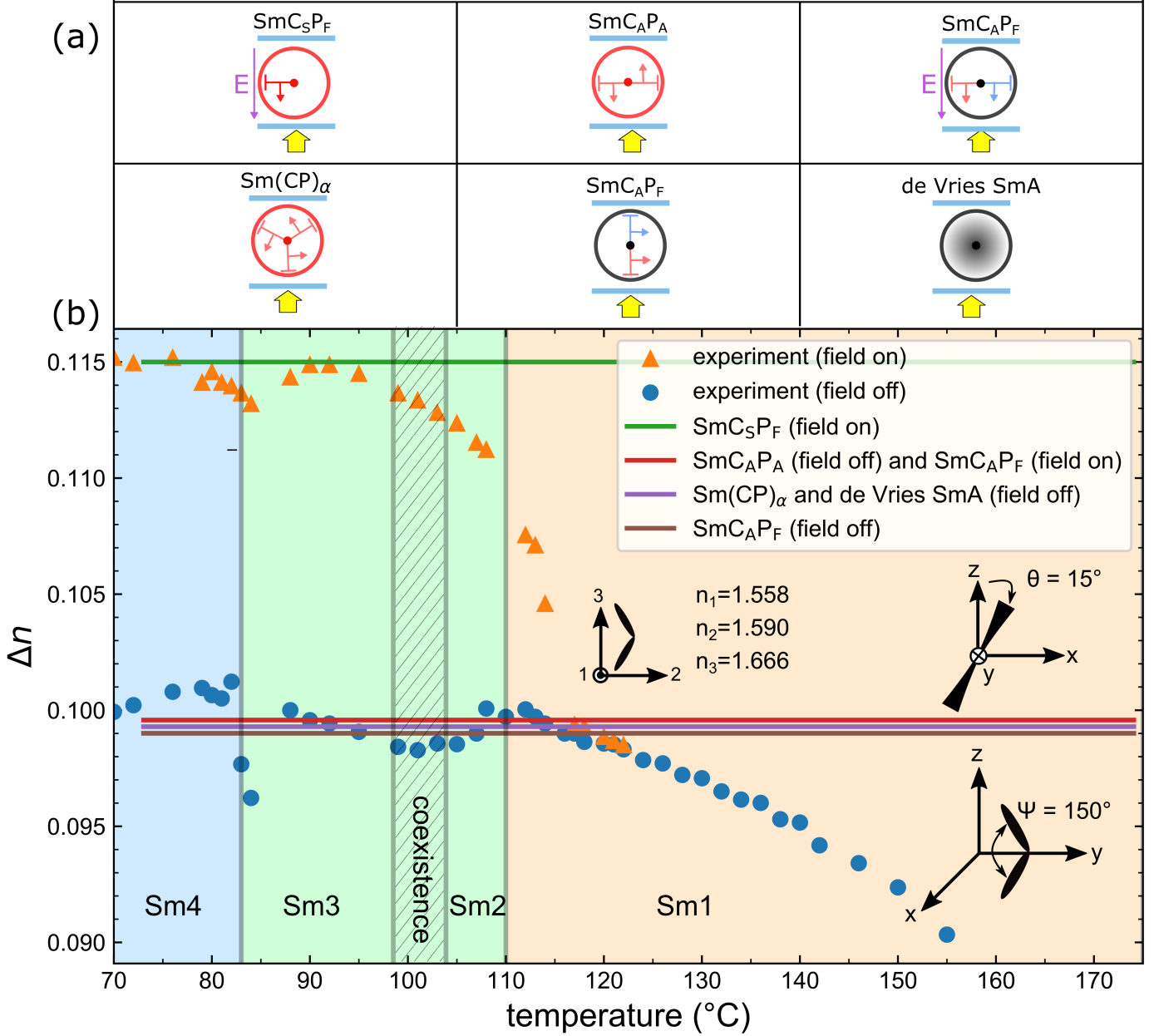


FIG. S6. The calculated birefringence for various model banana phases assuming an opening angle, $\Psi = 150^\circ$ and molecular tilt, $\theta = 15^\circ$ compared with the experimentally observed birefringence. (a) Schematic cross-sections of various smectic phases in a cell with bookshelf geometry. For chiral phases, the tilt-cone is red, while for achiral phases it is black. (b) Measured and calculated birefringence vs temperature. The birefringence is computed using indices of refraction chosen for the best fit to the experiment: $n_1 = 1.59$, $n_2 = 1.558$, $n_3 = 1.666$. The birefringence is computed using the method described by Shen *et al.* [5].

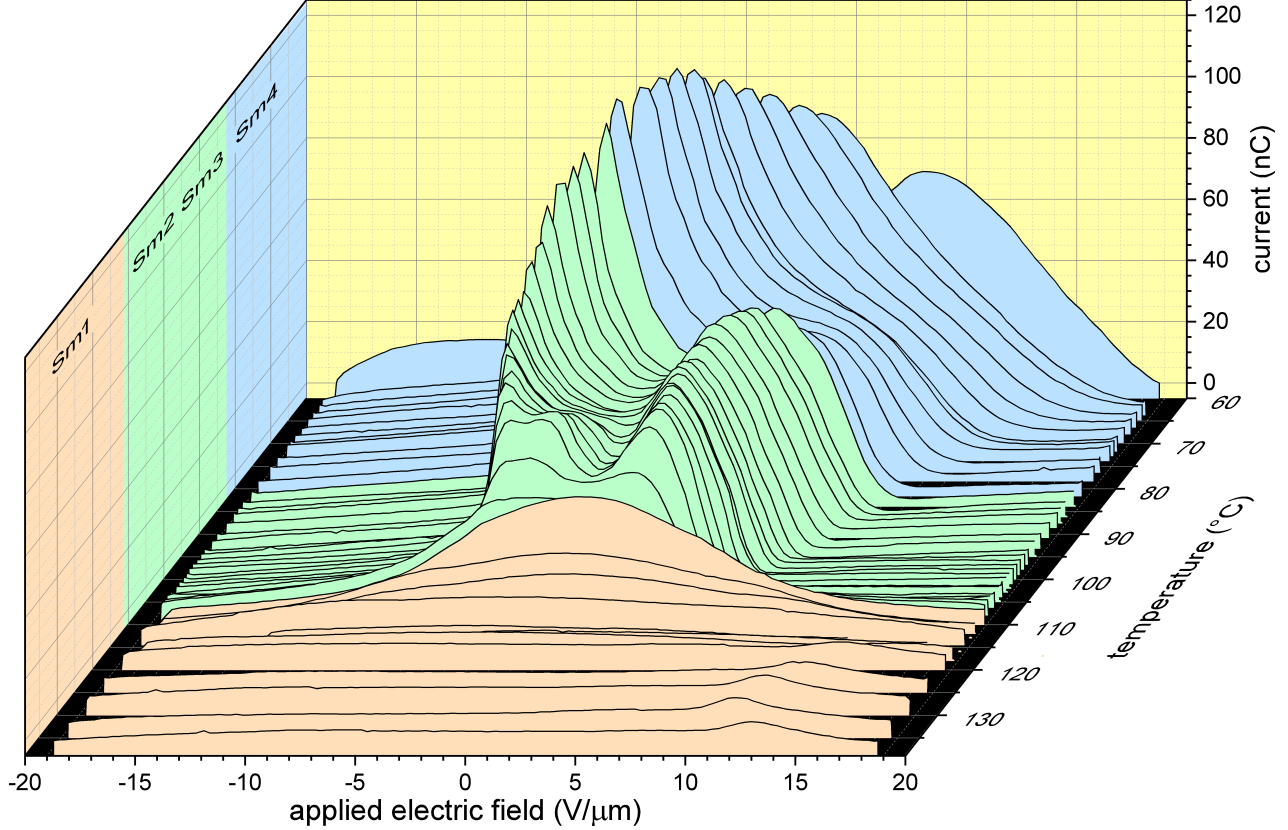


FIG. S7. Polarization current response of a 4.5 μm-thick **PAL30** sample in an Instec cell subjected to a 40 Hz triangular voltage with an amplitude of 72 V. The current response, $I = dP/dt$ in the Sm1 phase is a single, broad hump corresponding to the field-induced alignment of the initially random polarization. The Sm1 phase becomes a chiral Sm_{CSPF} when the polarization orientation saturates (when $I(V)$ goes to zero). As the temperature is lowered, this peak splits into sub-peaks, indicating internal stabilization of a state or states of lower polarization, which optical and RSoxS observation show to be the incommensurate Sm(CP) _{α} helix of SmCP layers in the Sm2 phase and bilayer Sm_{CAPA} antiferroelectric ordering of SmCP layers in the Sm3 phase. In the Sm2 phase, two current peaks appear during the rewinding of the helix as the magnitude of the applied field falls to zero. The right current peak (as the applied field increases again) marks the transition from the ground state of Sm(CP) _{α} to the field-aligned Sm_{CSPF}. Three polarization switching peaks are indicative of ferrielectricity (see the discussion of the Sm_{C^{*}FII} calamitic phase in Takezoe et al. [6]), and would be expected as the measured pitch of the Sm2 phase (2.8 layers) is close to the pitch of the quintessential ferrielectric phase, the Sm_{C^{*}FII} (3 layers). In the Sm3 phase, the left and right hand peaks mark the transitions from the Sm_{CSPF}-up to Sm_{CAPA}, and Sm_{CAPA} to Sm_{CSPF}-down, respectively. The transition to the Sm4 phase is marked by the appearance of a pattern of low birefringence (yellow) and high birefringence (orange) domains and a single current peak that moves continuously to $V = 0$, with a broad current 'shoulder' on the right. A current peak at $V = 0$ is characteristic of field-driven uniform, "block" reorientation of a ferroelectric polarization distribution, indicating the development of layer interactions that prefer Sm_{CAPF} over Sm_{CAPA}, the former being achiral as Figure 1(k-m) indicates. At zero field, the Sm_{CAPF} polarization is parallel to the glass, giving the low-birefringence, yellow domains seen in Figure 1(l). The orange domains remain from the field application (Figure 1(k)), indicating that these regions stay in the Sm_{CAPF}-up state until field reversal converts them into the Sm_{CAPF}-down state, also orange (Figure 1(m)). The 'shoulder' in this current peak results from the reorientation of these pinned domains. The liquid crystal phases are indicated schematically using the same color scheme as in Figure 1.

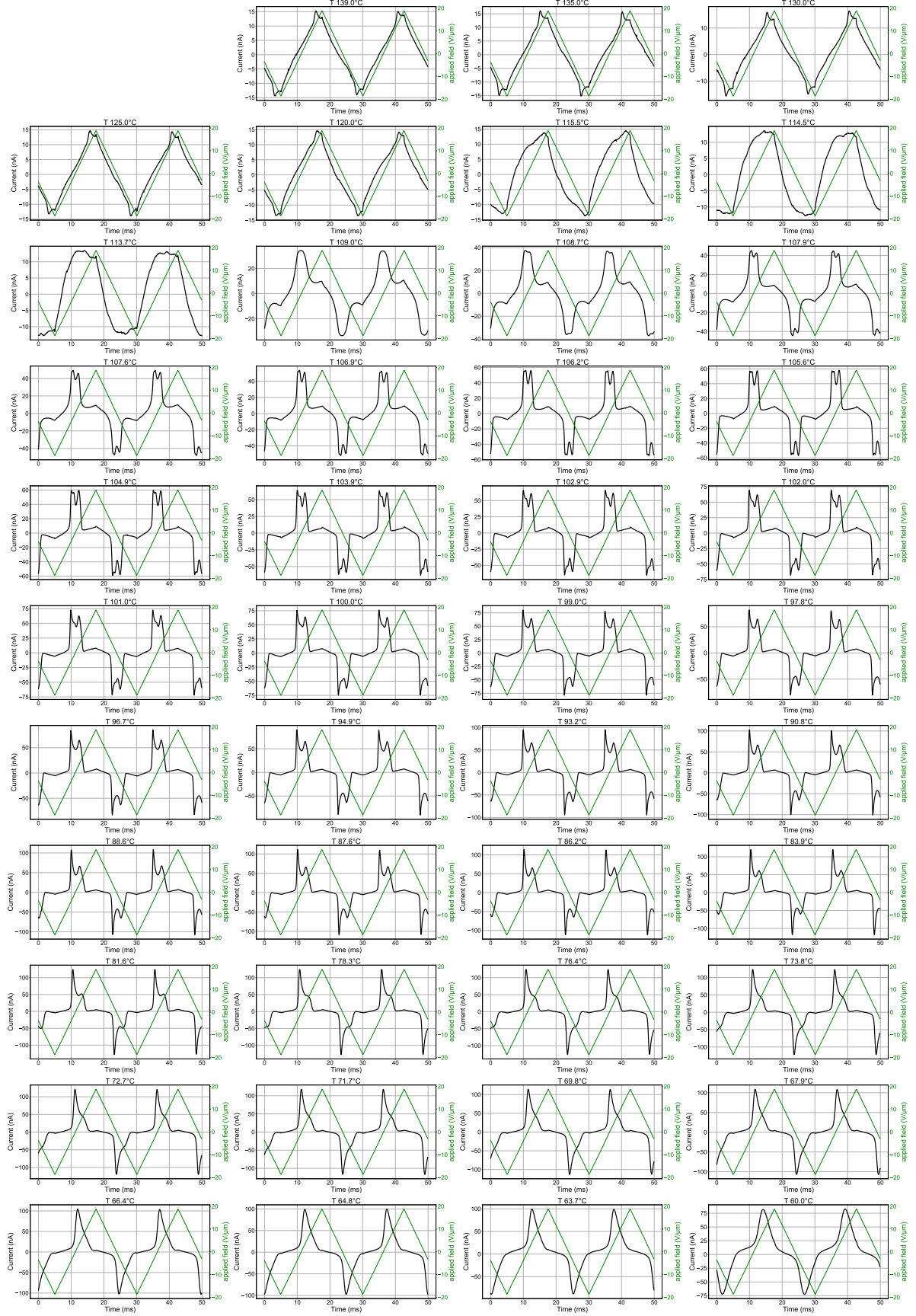


FIG. S8. Polarization current response vs. time of a 4.5 μm -thick **PAL30** sample in an Instec cell subjected to a 40 Hz triangular voltage with an amplitude of 72 V. The data are the same as in Figure S7.

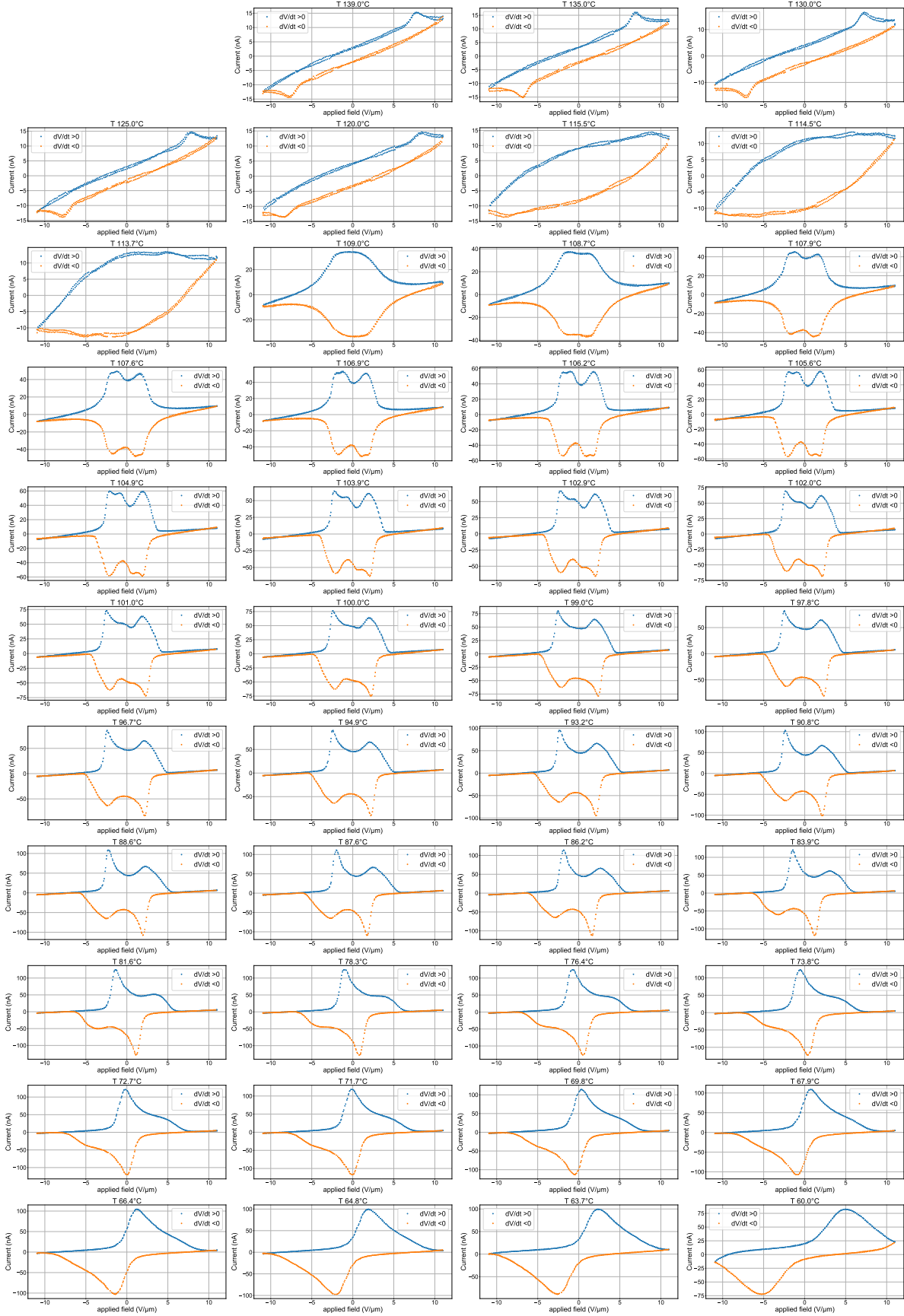


FIG. S9. Polarization current response vs. applied field of a $4.5\text{ }\mu\text{m}$ -thick **PAL30** sample in an Instec cell subjected to a 40 Hz triangular voltage with an amplitude of 72 V. The data are the same as in Figure S7. The blue and orange curves correspond respectively to the polarization current measured with an increasing and decreasing applied voltage.

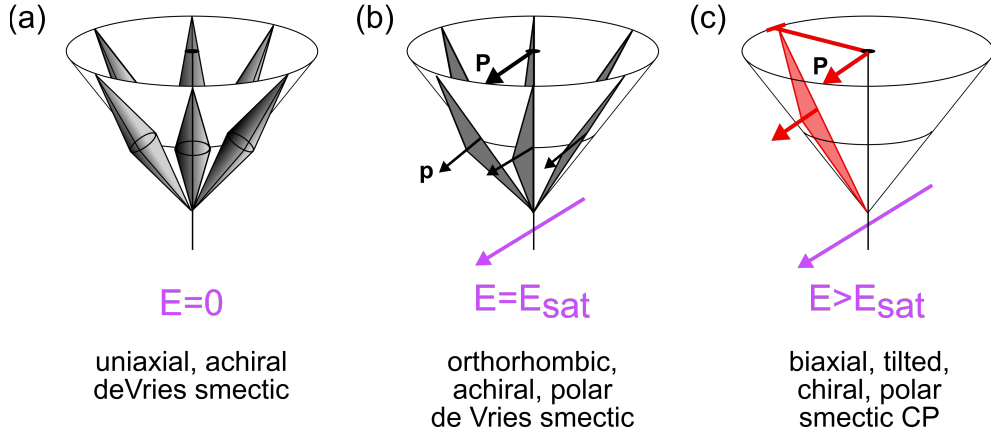


FIG. S10. Response of the Sm1 phase to an applied electric field. (a) At zero field, the Sm1 is a uniaxial, achiral de Vries smectic, where the tilt and polar order are azimuthally distributed. (b) Application of an electric field begins to align the polar director, though the tilt remains azimuthally distributed, giving a polar but achiral bent-core structure. (c) When the applied field is larger than the saturation value (E_{sat}), the tilt also aligns, giving a biaxial, tilted, polar and chiral bent-core structure.

-
- [1] C. Wang, D. H. Lee, A. Hexemer, M. I. Kim, W. Zhao, H. Hasegawa, H. Ade, and T. P. Russell, *Nano Lett.* **11**, 3906 (2011).
 [2] F. Liu, M. A. Brady, and C. Wang, *Eur. Polym. J.* **81**, 555 (2016).
 [3] J. Ilavsky, *J. Appl. Crystallogr.* **45**, 324 (2012).
 [4] F. Zhang, J. Ilavsky, G. G. Long, J. P. G. Quintana, A. J. Allen, and P. R. Jemian, *Metall. Mater. Trans. A* **41**, 1151 (2010).
 [5] Y. Shen, L. Wang, R. Shao, T. Gong, C. Zhu, H. Yang, J. E. MacLennan, D. M. Walba, and N. A. Clark, *Phys. Rev. E* **88**, 062504 (2013).
 [6] H. Takezoe, E. Gorecka, and M. Čepič, *Rev. Mod. Phys.* **82**, 897 (2010).